Medicon Engineering Themes
Volume 5 Issue 6 December 2023
Article Type: Research Article
ISSN: 2834-7218

Modeling of a Low-Power Wind Turbine with a Vertical Axis of Rotation within the Framework of the Comsol

Hamdamov MM*

Institute of Mechanics and Seismic Stability of Structures named after M.T.Urazbaev, AS RUz, Tashkent, Uzbekistan

***Corresponding Author:** Hamdamov MM, Institute of Mechanics and Seismic Stability of Structures named after M.T.Urazbaev, AS RUz, Tashkent, Uzbekistan.

Received: November 18, 2023; **Published:** December 04, 2023

Abstract

This paper presents the results of a k - ε turbulence model for a rectangular airfoil problem using standard Comsol Multiphysics solvers. Flow around a rectangular airfoil was studied at Reynolds numbers of 10 000 < Re < 2 000 000 and angle of attack α = 0°-20°. Results were obtained for speed, pressure and other parameters for different angle values. The implementation of the Comsol Multiphysics software package showed good convergence, stability and high accuracy of the model.

Keywords: Navier-Stokes equations; Comsol Multiphysics

In recent years, the Republic of Uzbekistan has adopted a set of measures aimed at further increasing the efficiency of the use of electrical energy in the sectors of the economy and in everyday life, the widespread introduction of energy-saving technologies and the development of renewable energy sources.

Over the past 50 years, 85% of the electricity generation in the republic corresponds to natural gas. The carbon dioxide and carbon oxides emitted as a result of the combustion of hydrocarbons lead to atmospheric pollution, a decrease in its transparency and an increase in turbidity. This, in turn, enhances the "greenhouse effect", which over the past hundred years has increased the average temperature of the Earth's atmosphere by 1.5-2 degrees. Such global climate change leads to the melting of the glaciers of the north and south poles of the Earth, the frequent formation of anomalous climatic phenomena. Ultimately, this is reflected in the global ecological state of the planet and the development of civilization. In this regard, today the widespread use of alternative sources of electricity is becoming relevant [1-5].

Of the alternative sources of electricity, the cheapest and most environmentally appropriate is the driving force of the wind, which has a high economic indicator.

In general, by 2030, the development of the total wind power capacity up to 5000 MW is predicted in Uzbekistan.

All this is about big energy. The government also supports small-scale power generation. Evidence of this judgment, in particular, is the financing, development and implementation of low-power wind turbines with a vertical axis of rotation.

The choice of a wind turbine with a vertical axis of rotation is justified by the fact that wind turbines with high power start working from 7 m/s wind speed. Such wind speeds in Central Asia are achieved at high altitudes, which is due to the areography of the area, or in certain regions, for example, in the Akhangaran valley, or in the coastal zones of the oceans. Thus, in the Republic of Uzbekistan, the wind potential refers to low wind speeds [6-10].

The second reason for choosing a wind turbine with a vertical axis of rotation is that such a design can operate with an arbitrary wind direction. When the wind direction changes, the horizontal axis of the wind turbine should be parallel to the wind direction. This is achieved either automatically, which requires additional capital investments, or manually, which requires additional operating costs.

Currently, software products are actively used in scientific and technical organizations and universities for modeling various processes. Their use in the study of heat engineering processes observed in engineering and technology has become relevant.

Vertical axis wind turbines have a simpler design than horizontal axis machines, and their lower blade speeds reduce safety and noise concerns. While vertical axis turbines do offer significant operational advantages, development has been hampered by the difficulty of modeling the aerodynamics involved as well as their rotating geometry. This paper presents simulation results of a basic vertical axis wind turbine calculated using the commercial finite volume code Star-CCM+ and compares them with data obtained from a multi-flow tube model. Emphasis was placed on the dynamic characteristics of stall and wake formation, which have the greatest impact on turbine performance. A model was developed to reproduce the blade-wake interaction characteristic of higher tip speeds and was found to significantly improve the accuracy of the blade-element momentum model [14].

Two rectangular orifice wing models were designed and tested in the Duke University wind tunnel to better understand the effects of damage. A rectangular hole is used to simulate damage. A wing with a hole is structurally modeled with a thin elastic plate using the finite element method. The unsteady aerodynamics of a plate wing with an opening is modeled using the doublet lattice method. The equations of aeroelastic motion are derived using the Lagrange equation. The flutter boundary is found using the V-g method. The location of the opening affects the mass, stiffness, aerodynamics and therefore the aeroelastic properties of the wing. Linear theoretical models have been shown to be able to predict critical speed and flutter frequency, confirmed by wind tunnel tests [15].

Turbulent separated flows play an important role in modern aerodynamics due to the need to analyze non-standard flight conditions and solve a number of other problems inextricably linked with the phenomenon of flow separation from a streamlined surface. The complexity of modeling separated flows is explained by their physical features, the parameters of which are determined by the specific geometric characteristics of the flow under consideration and boundary conditions, which makes the construction of a universal semi-empirical turbulence model for calculating separated flows extremely difficult. It is known that numerical modeling of separated flows can be performed on the basis of various turbulence models and even on an ideal fluid model, where the effects of energy dissipation are created by numerical diffusion. It has also been repeatedly noted in the literature that due to numerical diffusion it is possible to simulate the effects of turbulence, while improving the convergence and stability of the mathematical calculation [11-13].

Hydrodynamic singularity methods, which use the distribution of singularities over the surface of an aircraft, have found wide application in the calculation of complex spatial flows. The flow parameters at a given point are determined by integrating 42 disturbances from all features. This integration is carried out numerically [15, 16]. If you select a final section of the surface, then under certain conditions you can analytically integrate the influence of features located on the selected section. In this case, we come to the panel calculation method. Panel methods are convenient, for example, when considering local variations in the surface of an aircraft. Then, on panels not included in the modification zone, the integration of disturbances can be carried out only once for the original version, which saves calculation time on an electronic computer (computer). However, the analytical calculation of integrals of distributed features imposes restrictions on the shape of the panel and the type of approximation of the feature density distribution function. For example, in the known method [17], the wing panels must have parallel side edges and be flat. These requirements lead to a significant schematization of the surface of the aircraft at the interfaces of the layout elements. The software package [18, 19] uses arbitrary quadrangular panels in the form of elements of a hyperbolic surface with a quadratic dipole distribution. The disturbance fields from such panels are described by complex analytical expressions, which require significant time resources when calculating on a computer.

When distributing vortices and sources over the surface of load-bearing elements, the principle of symmetrization of features proposed in [20] is used to calculate the flow around profiles. Here this principle is extended to the three-dimensional case. Let us first consider the well-known method for calculating the flow around solid wings with linearization of the boundary conditions [17]. In this method, a layer of sources and vortices was located in the base plane of the wing. The density of the sources was set to be proportional

to the slopes of the half-thickness line of the profiles, and the circulation of the vortex layer was determined from the condition of non-flow of the middle surface of the wing. Let's divide the layer of sources and vortices into two equal parts and place these parts on the upper and lower surfaces of the wing. The intensity of the sources and vortices will be determined from the non-flow conditions, which will be satisfied at the control points of the panels distributed over the surface of the wing. Naturally, the number of panels on the top and bottom surfaces should be the same, 44, but the sizes of the panels may differ. Let us recall that the density distribution of vortices is piecewise linear, and that of sources is piecewise constant. Just like in all panel methods, the problem is reduced to solving a system of linear equations for unknown intensities of features [17-20]. After solving the system, the velocities at the control points of the panels are calculated, the pressure values and the total aerodynamic characteristics are determined.

The method of symmetrical singularities allows you to calculate both thin and thick wings. In the limiting case of an infinitely thin lifting surface, it continuously transforms into the well-known calculation scheme with the distribution of vortices over the middle surface of the wing. In this case, the source layer degenerates and its intensity tends to zero.

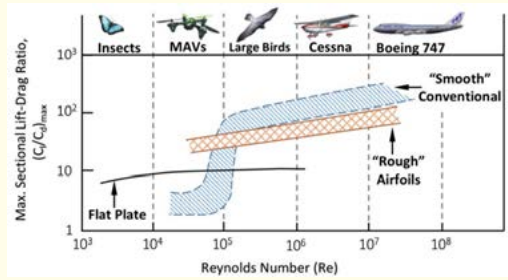

Figure 1: The influence of the Reynolds number on the maximum aerodynamic efficiency of the profile section.

The finite element method was used to numerically solve the system of initial unsteady equations and the k - ε turbulence model. Standard COMSOL Multiphysics 6.1 solvers were used for the solution.

Wind energy is a low-density energy source. Maximizing the efficiency of converting wind energy into mechanical forms of energy is critical to ensuring the economic efficiency of wind. Knowledge and understanding of rotor aerodynamics and blade shape design improves the overall performance of modern turbines. Wind turbine technology is based on the distribution of forces on the turbine rotor blades 3, caused by the mechanical torque on the shaft.

The shaft transmits torque from the blades to the generator. In modern wind turbines, the aerodynamic driving force is primarily lift, rather than drag, as in ancient sailing ships.

Research conducted in this area has led to significant improvements in the overall efficiency of the energy conversion process. The ability to predict the updrafts of the flow field is an important factor determining the interaction between turbines. Three approaches are available to analyze the flow around and downstream of wind turbines [14]:

Field tests; it gives accurate results, but is very complex and expensive;

Analytical and semi-empirical models, which make simplistic assumptions and are therefore not universally reliable;

Computational fluid dynamics (CFD) offers a better alternative to direct measurements.

The purpose of this work is to study the aerodynamics of a vertical axis wind turbine blade by numerically solving the governing equations using the finite volume method and the averaged Reynolds Navier-Stokes method.

Physico-mathematical formulation of the problem

A two-dimensional turbulent flow around a rectangular profile is considered. The physical picture of the flow under study and the configuration of the calculated fields are shown in Fig. 2.

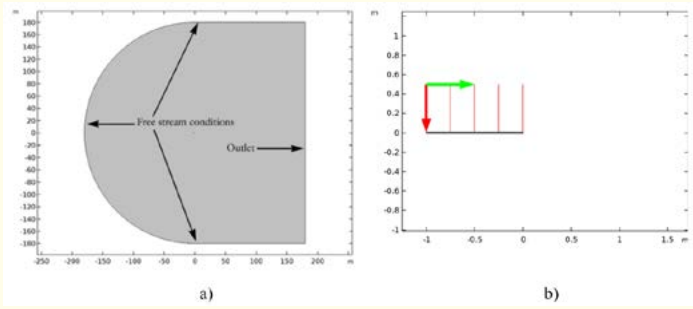

Figure 2: Scheme of computational domains: a) flow around the profile b) profile geometry.

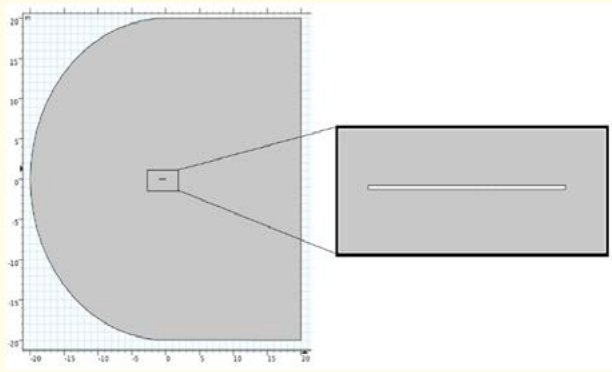

Figure 3: Profile geometry.

For a rectangular profile problem, the Reynolds number based on chord length is $10000<Re<2*10^6$. Chord length $c=1\ m$. Two options for the angle of attack of the profile from a=0 to a=20 are considered.

Conservation equations. The general mass conservation equation or continuity equation can be written as follows (1).

$$\frac{d\rho}{dt}+\nabla\left(\rho\vec{v}\right)=0 \qquad (1)$$

where ρ liquid density and $\vec{v}$ - velocity vector.

Equation of conservation of momentum. The general equation can be written as follows (2):

$$\frac{d}{dt}\left(\rho\vec{v}\right)+\nabla\left(\rho\vec{v}\right)=-\nabla_p+\nabla\overline{\overline{T}}+\rho g+F \qquad (2)$$

where p — static pressure, g and F — the force of the gravitational body and the external forces of the body (for example, arising during interaction with the dispersed phase), respectively.

Stress tensor $\overline{\overline{\tau}}$ in the following form (3):

$$\overline{\overline{\tau}} = \mu\left[\left(\nabla\vec{v} + \nabla\vec{v}T - \frac{2}{3}\nabla\vec{v}I\right)\right] \qquad (3)$$

where μ — molecular viscosity, a I — unit tensor.

Reynolds and Navier-Stokes equations

The Reynolds-averaged Navier-Stokes (RANS) equations are time-averaged equations of motion for fluid flow. They are mainly used when working with turbulent flows. These equations can be used with approximations based on knowledge of the flow turbulence properties to obtain approximate average solutions of the Navier-Stokes equations. The equations can be written in Cartesian tensor form as (4), (5):

$$\frac{d\rho}{dt} + \frac{d}{dx_i}\left(\rho\vec{v}_i\right) = 0 \qquad (4)$$

$$\frac{d}{dt}\left(\rho\vec{v}_i\right) + \frac{d}{dx_i}\left(\rho v_i v_j\right) = -\frac{dp}{dx_i} + \frac{d}{dx_j}\left[\mu\left(\frac{dv_i}{dx_i} + \frac{dv_j}{dx_j} - \frac{2}{3}\delta_{ij}\frac{dv_i}{dx_j}\right)\right] + \frac{d}{dx_i}\left(-\rho v_i v_j\right) \qquad (5)$$

Equations (4) and (5) are called Reynolds-averaged Navier-Stokes equations, in which the velocities and other decision variables are now ensemble averages (or time averages). Given fluid velocity as a function of position and time, the average fluid velocity (6):

$$v_i = v_i + v_i' \qquad (6)$$

The left frequency equation represents the change in the average momentum of the mass element due to the unsteadiness of both the average flow and convection to the average flow.

Laminar flows are characterized by low Reynolds numbers. The higher the Reynolds number, the more likely the flow is to be turbulent, and the less shallow lengths (mixing) there are in the flow. The Reynolds number gives a measure of the relative importance of inertial and viscous forces; for a wing it is defined as:

To find out whether the flow is steady or turbulent, we need to calculate the Reynolds number

$$\mathrm{Re} = \frac{\rho u l}{\mu} = \frac{1.2043 \times 20 \times 1}{1.81397 \times 10^{-5}} = 1.327805 \times 10^{6}$$

As can be seen from this Re value, the turbulence becomes very large. Therefore, we should select a turbulent model that represents this process and use it for this problem.

Mathematical model of turbulence

Comsol provides the following capabilities for turbulence models.

Spalart-Almaras model;
k - ε models (standard, renormalization group (RGG), realizable);
k - ω models (standard stress transformation (SST));
Transitional SST models;

Reynolds Stress Models (RSM);
Eddy Simulation Model (DES);
Large eddy simulation (LES) model.

Standard k-e model: It has good stability and accuracy under high turbulent Reynolds number flow conditions, but is not suitable for rotation effect simulation;

RNG k - ε model: It can be used for low Reynolds numbers because the simulation accuracy will increase with fast deformation flow due to the rotation effect;

Implementable k - ε model: it is more accurate for predicting the acceleration rate of both flat and round jets, but produces unphysical turbulent viscosity when the model being simulated includes both a rotating and stationary fluid zone;

Standard k - ω model: It contains the effects of low Reynolds ratio, compressibility and shear flow propagation. It agrees well with measurements with problems of far wake, layer mixing, and flat, circular, and radial jets;

Shear Model (SST) k-ω: Because it combines both the good near-wall accuracy of the standard k-ω model and the good accuracy of the far-field k-e model (Fluent 01 User Manual 5/12/2006), it is more accurate and reliable for a wider class of flow than the standard k-ω model;

Reynolds Stress Model: By eliminating the eddy viscosity hypothesis, the Reynolds Stress Model (RSM) directly calculates Reynolds stresses. Theatrically, this is much more accurate than the k - ε and k - ω models, but five additional transport equations in 2D streams and seven additional transport equations in 3D streams [14-16] take up enormous computer resources. and long simulation. fixed time.

The choice of turbulence model will depend on considerations such as the physics of the flow, established practice for a given class of problems, the level of accuracy required, the computational resources available, and the amount of time available for the simulation.

To make the most appropriate model selection for your application, you need to understand the capabilities and limitations of the various options.

Flow turbulence effect

The presence of turbulent flows significantly depends on the presence of walls. Obviously, the average velocity field is affected by the non-slip condition that must be satisfied on the wall.

However, turbulence is also modified by the presence of a wall in non-trivial ways. Very close to the wall, viscous damping reduces tangential velocity and kinematic locking reduces normal vibrations. However, towards the outer part of the near-surface region, turbulence increases rapidly due to the creation of turbulent kinetic energy due to large average velocity gradients [10-15].

The k-e, RSM, and LES models are primarily valid for turbulent core flows (i.e., flows in regions somewhat distant from the walls). Therefore, it is necessary to consider how to make these models suitable for wall flows. The Spalart-Allmaras and k - ω models were designed to be applied to the entire boundary layer, provided that the grid wall resolution is sufficient. In this simulation study, a turbulent k - ε model with a standard wall function was used.

The reason for this choice is the close-wall grating resolution of the generated mesh. The k-e turbulence model is one of the most common models. It is a two-equation model that includes two additional transport equations to represent the turbulent properties of fluid flows. However, the SST k-ω model was also used in simulations that did not produce realistic results and therefore were not consistent with the current model.

Modified model k - ε

Unlike well-known works, here it is proposed to use a modified *k* - *ε* model, which contributes to a more adequate description of the heat and mass transfer process [15-19]:

$$\begin{cases} \frac{\partial}{\partial t}(\rho k)+\frac{\partial}{\partial x_j}(\rho k u_j)=\frac{\partial}{\partial x_j}\left[\left(\mu+\frac{\mu_t}{\sigma_k}\right)\frac{\partial k}{\partial x_j}\right]+G_k+G_b-\rho\varepsilon-2\rho\varepsilon M_t^2+S_k, \\ \frac{\partial}{\partial t}(\rho \varepsilon)+\frac{\partial}{\partial x_j}(\rho \varepsilon u_j)=\frac{\partial}{\partial x_j}\left[\left(\mu+\frac{\mu_t}{\sigma_\varepsilon}\right)\frac{\partial \varepsilon}{\partial x_j}\right]+\rho C_1 S\varepsilon-\rho C_2\frac{\varepsilon^2}{k+\sqrt{\nu\varepsilon}}+C_{1\varepsilon}\frac{\varepsilon}{k}C_{3\varepsilon}G_b+S_\varepsilon. \end{cases}$$

The notation used here is

$$C_1=\max\left[0.43,\frac{\eta}{\eta+5}\right],\quad \eta=S\frac{k}{\varepsilon},\quad S=\sqrt{2S_{ij}S_{ij}},\quad \mu_t=\rho C_\mu\frac{k^2}{\varepsilon},\quad C_\mu=\frac{1}{A_0+A_S\frac{kU^*}{\varepsilon}},$$

$$U^*=\sqrt{S_{ij}S_{ij}+\tilde{\Omega}_{ij}\tilde{\Omega}_{ij}},\quad \Omega_{ij}=\overline{\Omega_{ij}}-2\varepsilon_{ijk}\omega_k,\quad A_S=\sqrt{6}\cos\phi,\quad \phi=\frac{1}{3}\cos^{-1}\left(\sqrt{6}W\right),\quad W=\frac{S_{ij}S_{jk}S_{ki}}{\tilde{S}^3},$$

$$\tilde{S}=\sqrt{S_{ij}S_{ij}},\quad S_{ij}=\frac{1}{2}\left(\frac{\partial u_j}{\partial x_i}+\frac{\partial u_i}{\partial x_j}\right),\quad G_k=-\rho\overline{u_i'u_j'}\frac{\partial u_j}{\partial u_i},\quad S=\sqrt{2S_{ij}S_{ij}},\quad G_b=\beta g_i\frac{\mu_t\partial T}{\mathrm{Pr}_t\partial x_i},\quad \mathrm{Pr}_t=1/a_t,$$

$$a_0=1/\mathrm{Pr}=k/\mu c_p,\ \beta=-\frac{1}{\rho}\left(\frac{\partial\rho}{\partial T}\right)_p,\ G_b=-g_i\frac{\mu_t}{\rho\,\mathrm{Pr}_t}\frac{\partial\rho}{\partial x_i},\ M_t=\sqrt{\frac{k}{a^2}},\ a=\sqrt{\gamma RT}.$$

Empirical constants *k* - *ε* models take standard values: $C_{1\varepsilon}=1.44,\ C_2=1.9,\ \sigma_k=1.0,\ \sigma_\varepsilon=1.2,\ A_0=4.04$.

The *k* - *ε* model is apparently the most successful model of first-level closure turbulence. To describe turbulent quantities, it uses a system of two nonlinear diffusion equations - for the mass density of turbulent energy k and the dissipation rate of turbulent energy *ε*. The simplest version of this model appeared more than thirty years ago. Since then, the k-ε model has been widely used to calculate a wide range of problems, mainly to describe shear incompressible turbulence.

Spalart-Allmaras model

This model belongs to the class of one-parameter linear turbulence models. Here only one additional differential equation appears for calculating the kinematic coefficient of eddy viscosity. This low Reynolds turbulence model, which describes the entire flow region, is given by the following equation:

$$\frac{\partial}{\partial t}(\rho\tilde{\nu})+\frac{\partial}{\partial x_i}(\rho\tilde{\nu}u_i)=$$

$$G_\nu+\frac{1}{\sigma_{\tilde{\nu}}}\left[\frac{\partial}{\partial x_j}\left\{(\mu+\rho\tilde{\nu})\frac{\partial\tilde{\nu}}{\partial x_j}\right\}+C_{b2\rho}\left(\frac{\partial\tilde{\nu}}{\partial x_j}\right)^2\right]-C_{w1\rho}f_w\left(\frac{\tilde{\nu}}{d}\right)^2+S_{\tilde{\nu}}.$$

Turbulent eddy viscosity is calculated by the formula: $\mu_t=\rho\tilde{\nu}f_{\nu1}$, additional definitions are given by the following dependencies: $f_{\nu1}=\frac{\chi^3}{\chi^3+C_{\nu1}^3},\ \chi=\frac{\tilde{\nu}}{\nu},\ \tilde{S}\equiv S+\frac{\nu}{\kappa^2d^2}f_{\nu2},\ f_{\nu2}=1-\frac{\chi}{1+\chi f_{\nu1}},\ S\equiv\sqrt{2\Omega_{ij}\Omega_{ij}},\ \Omega_{ij}=\frac{1}{2}\left(\frac{\partial u_i}{\partial x_j}-\frac{\partial u_j}{\partial x_i}\right),\ S_{ij}=\frac{1}{2}\left(\frac{\partial u_j}{\partial x_i}+\frac{\partial u_i}{\partial x_j}\right),$

$f_w = g\left[\frac{1+C_{w3}^6}{g^6+C_{w3}^6}\right]^{1/6}$, $r = \frac{\tilde{\nu}}{\tilde{S}\kappa^2 d^2}$ and the closure constants for the model are: $C_{prod} = 2.0$, $C_{b1} = 0.1355$, $C_{b2} = 0.622$, $\sigma_{\tilde{\nu}} = \frac{2}{3}$, $C_{\nu 1} = 7.1$, $C_{w1} = \frac{C_{b1}}{\kappa^2} + \frac{(1+C_{b2})}{\sigma_{\tilde{\nu}}}$, $C_{w2} = 0.3$, $C_{w3} = 2.0$, $\kappa = 0.4187$.

Calculation grids

In this work, a thickening of the mesh was used near the surface of the profile shown in Fig. 4.

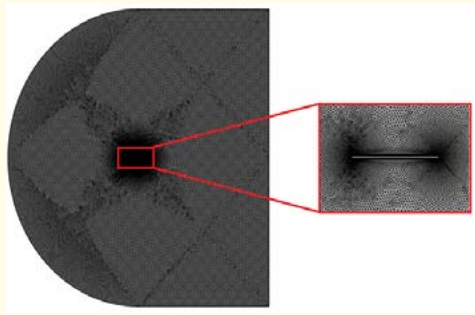

Figure 4: Calculation mesh of flow around the profile.

For the flow around the profile, a computational mesh of size 60300 was used. For the system of equations (1), obvious boundary conditions for adhesion on solid walls are specified. The output accepts extrapolation conditions for all parameters. At the inlet, uniform profiles of the longitudinal velocity component are used with $V_x = U_0$, the transverse component of velocity and pressure were assumed to be zero $V_y = P = 0$. The values of relative velocities (disturbances) are also supplied to the input: $\vartheta_x = 0.004$, $\vartheta_y = 0$.

The initial data for calculating the dimensional parameters are: wind speed m/s, angular velocity rad/s, air density, kg/m^3.

Label: Parameters 1

Parameters

Name	Expression	Value	Description
U_inf	20[m*s^-1]	20 m/s	Free-stream velocity
rho_inf	1.2043[kg*m^-3]	1.2043 kg/m³	Free-stream density
mu_inf	1.81397e-5[kg*m^-1*s^-1]	1.814E-5 kg/(...	Free-stream dynamic vis...
L	20[m]	20 m	Domain reference length
c	1[m]	1 m	Chord length
k_inf	0.1*mu_inf*U_inf/(rho_inf*L)	1.5062E-6 m²/s²	Free-stream turbulent kin...
om_inf	10*U_inf/L	10 1/s	Free-stream specific dissi...
alpha	0	0	Angle of attack
Re	U_inf*c*rho_inf/mu_inf	1.3278E6	

Solution method

Time-averaged and normalized longitudinal velocity (or flow velocity) profiles allow the flow characteristics to be assessed at various points downstream of the profile. Profile normalization means that the flow values at each point are divided by the maximum flow value in that profile. Time-averaged and normalized longitudinal velocity profiles are evaluated at three points (x/c = 0, 0.25, 0.5, 0.75, and 1) behind the profile.

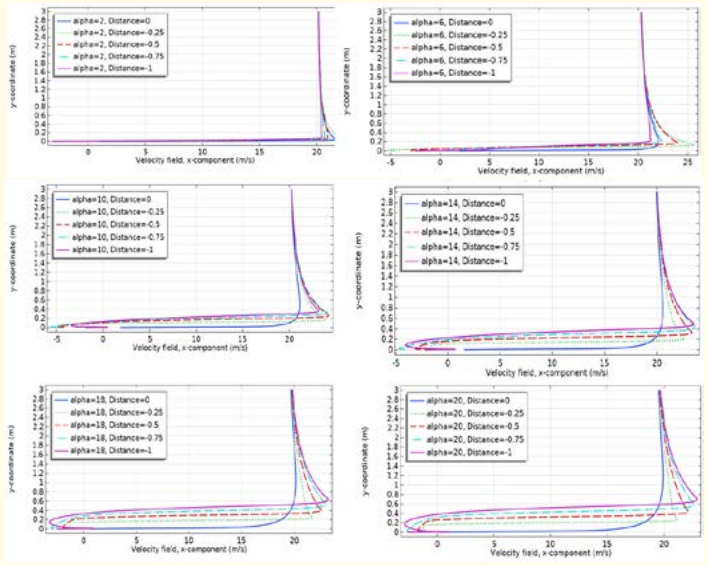

Figure 5: Longitudinal velocity field at sections x/c = 0, 0.25, 0.5, 0.75,1.

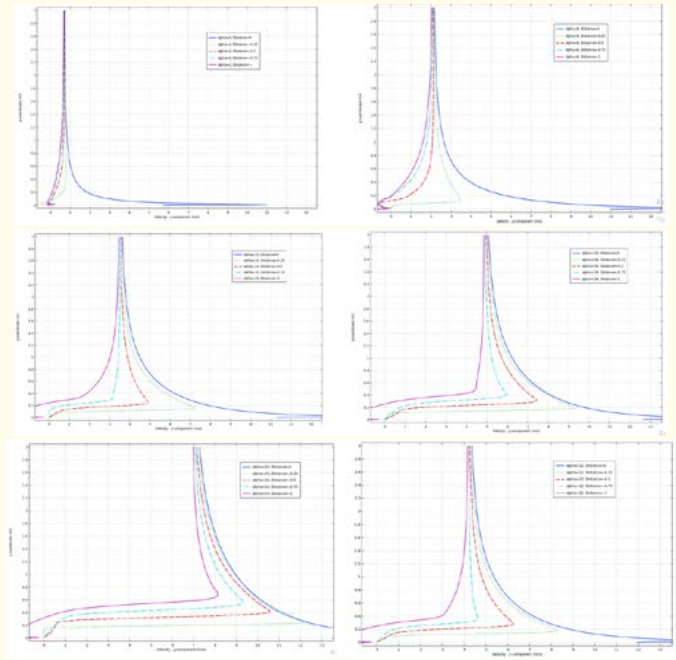

Figure 6: Transverse velocity field at sections x/c = 0, 0.25, 0.5, 0.75,1.

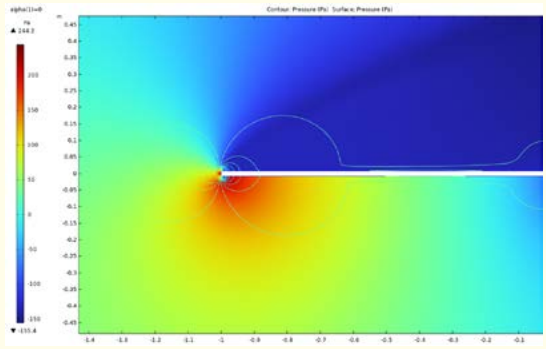

Figure 7: Pressure field at alpha = 0 deg.

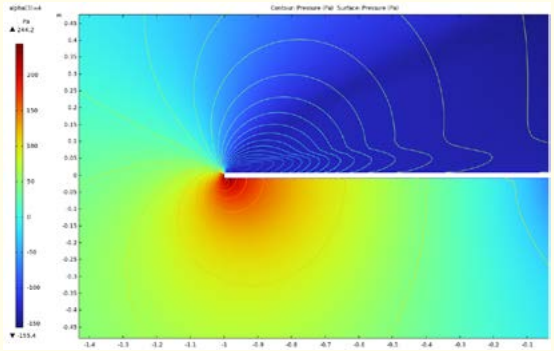

Figure 8: Pressure field at alpha= 4 degrees.

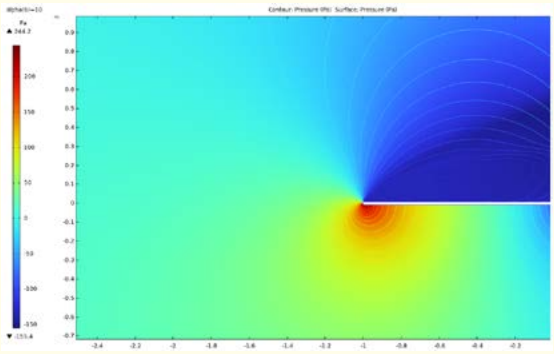

Figure 9: Pressure field at alpha = 10 degrees.

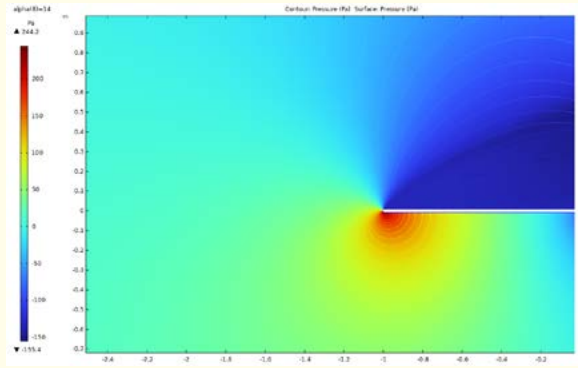

Figure 10: Pressure field at alpha = 14 degrees.

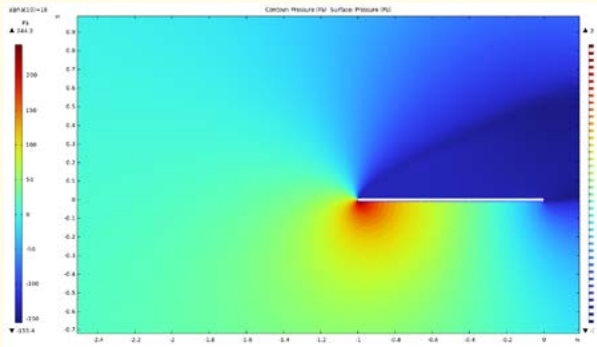

Figure 11: Pressure field at alpha = 18 degrees.

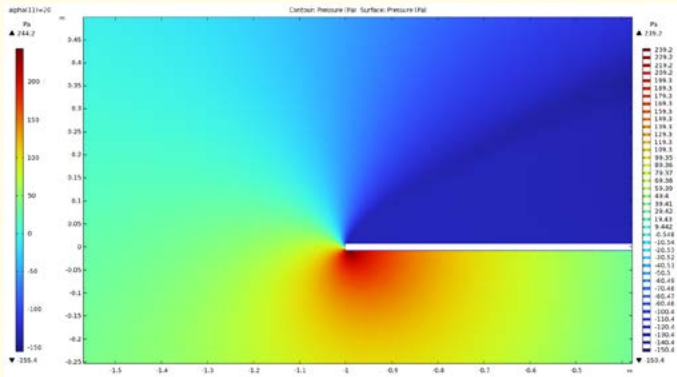

Figure 12: Pressure field at alpha = 20 degrees.

The distribution of the surface pressure coefficient on the wing profile is characterized by a change in pressure on its surface depending on the distance from a certain point. Typically the analysis uses the surface pressure coefficient (Cp), which is defined as the ratio of the pressure difference between a point on the profile surface and the free flow pressure to the dynamic free flow pressure.

$$C_p = \frac{p - p_\infty}{0.5\rho U_0^2}$$

where p — pressure at a point on the profile surface, P_∞ — free stream pressure, ρ — free stream density, U_0 — free stream speed.

On the charts C_p zones of positive and negative pressure are usually distinguished. The positive pressure zone is usually called the lift zone, and the negative pressure zone is called the resistance zone. The distribution of the surface pressure coefficient on the wing profile can be used to analyze its aerodynamic characteristics, such as lift, drag coefficient, etc. Fig. 13 - shows the distribution of the surface pressure coefficient Cp at angles of attack $\alpha = 0^0 \ldots\ldots 20^0$.

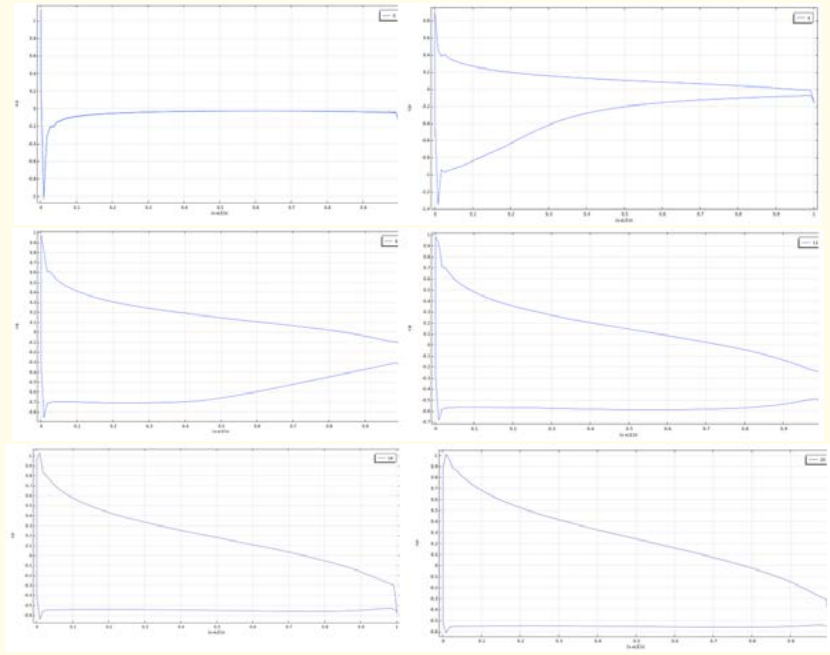

Figure 13: Surface pressure coefficient Cp.

The distribution of the surface friction coefficient on an airfoil is characterized by a change in the friction force on its surface depending on the distance from a certain point.

The influence of the accuracy of boundary layer modeling on the accuracy of calculating the integral and distributed characteristics of the wing profile is studied using the RAE 2822 as an example. Two mathematical models of gas flow are used: k-ω SST and "inviscous" gas. The solution is carried out by algorithms of the first and second orders of accuracy, which give different results in the region of boundary layer separation. As numerical studies have shown, the accuracy of calculating the friction coefficient on the surface of the profile and the thickness of the boundary layer significantly affects the determination of the flow separation point, which affects the calculation of the pressure distributed over the surface and the integral characteristics of the profile [16-23].

The coefficient of surface friction C_f is defined as the ratio of the friction force acting on the surface of the profile to the dynamic pressure of the free flow.

$$C_f = \frac{F}{0.5\rho U_0^2 S}$$

where F is the friction force acting on the profile surface, S is the profile surface area oriented along the flow. To analyze the distribution of the surface friction coefficient on the wing profile, graphs of Cf are usually used depending on the distance from a certain point on the profile surface. On Cf graphs, zones of high and low friction are usually distinguished. The high friction zone is usually located in the area of the leading edge of the profile and in the area of flow separation on the upper surface of the profile, as can be seen in Fig. 14.

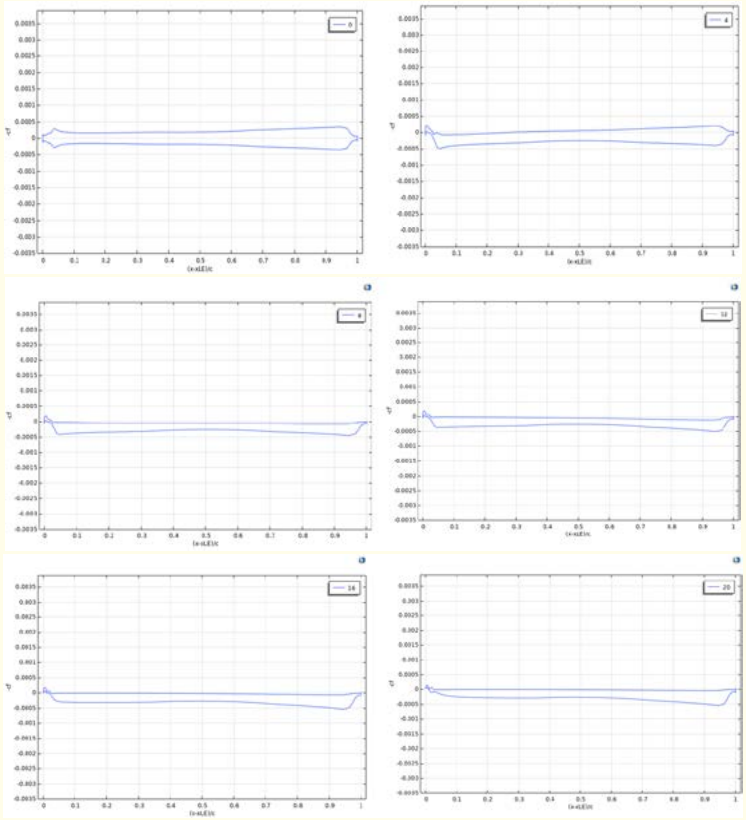

Figure 14: Surface friction coefficient Cf.

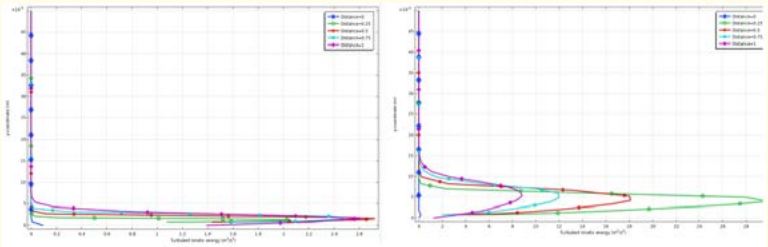

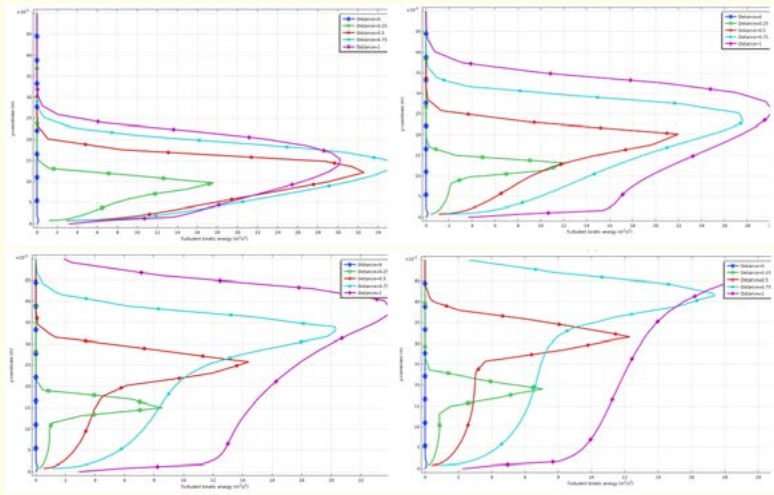

Figure 15: Kinetic energy of turbulence.

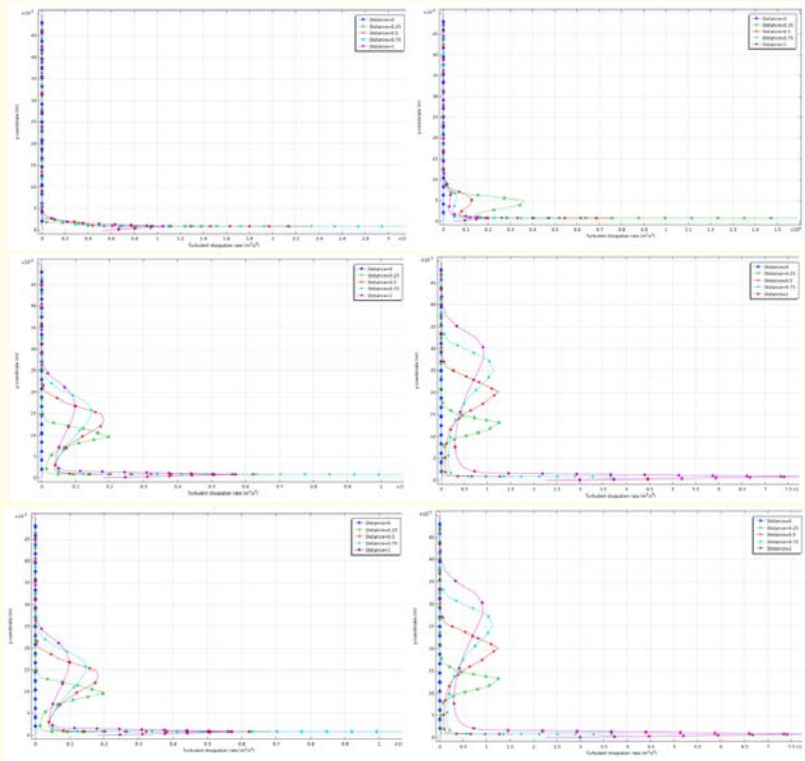

Figure 16: Dissipation of turbulence energy.

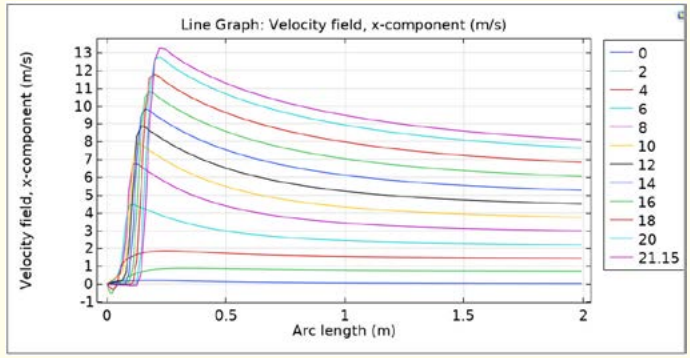

Figure 17: Velocity field at different alpha values.

Conclusion

The article presents numerical results of turbulent flow of an incompressible fluid around a rectangular profile using the k - ε turbulence model in the Comsol Multiphysics software package.

The accuracy of determining the separation point of the boundary layer depends on the reliability of modeling friction stresses on the wall; an erroneous determination leads to a distortion of the pressure coefficient and leads to errors in the integral characteristics. But, as practice shows, it is not always necessary to pay much attention to the accuracy of determining friction stresses. With continuous flow, its influence is small, and, consequently, the choice of the model with which to solve the problem is significantly easier.

References

1. J Liu, H Lin and J Zhang. "Review on the technical perspectives and commercial viability of vertical axis wind turbines". Ocean Eng 182 (2019): 608-626.
2. Solovyov Alexander. Degtyarev Kirill. Wind energy. Science and life (2013).
3. Energy portal. Issues of production, conservation and processing of energy (2022).
4. Obukhov SG. Electricity Generation Systems Using Renewable Energy Resources: Textbook. - Publishing House of Tomsk State University (2008).
5. Martyanov AS. Research of control algorithms and development of a controller for a wind power plant with a vertical axis of rotation: diss ... cand. tech. Sciences. - Chelyabinsk (2016).
6. Mezaal NA. Mathematical modeling of a wind power plant (WPP) with a capacity of 1.5 MW using computational fluid dynamics (CFD) in ANSYS: Master's thesis. - Chelyabinsk: SUSU (2018).
7. D MacPhee and A Beyene. "Recent advances in rotor design of vertical axis wind turbines". Wind Eng 36.6 (2012): 647-666.
8. Versteeg HK and W Malalasekera. An introduction to computational fluid dynamics: the finite volume method. 2007: Pearson education.
9. Oganesyan EV, Bekirov EA and Asanov MM. "Mathematical model for determining the operating parameters of a wind power plant". Construction and industrial safety 3.55 (2016): 82-86.
10. Kaplya YeV. "Mathematical model of transient processes of a rotatingly dangerous wind power plant". Math. modeling (2013).
11. Belotserkovsky OM. "Large particle method in gas dynamics". O.M. Belotserkovsky, Yu.M. Davydov. -M: Science (1982).
12. Fletcher K. Computational methods in fluid dynamics: In 2 vols.: trans. from English K. Fletcher. -M: Peace (1991).
13. Peter A Kozak., et al. "Modeling Vertical-Axis Wind-Turbine Performance: Blade-Element Method Versus Finite Volume Approach". Journal of Propulsion and Power 32.3 (2016).

14. Howard J Conyers, Earl H Dowell and Kenneth C. Aeroelastic Studies of a Rectangular Wing with a Hole: Correlation of Theory and Experiment Hall Department of Mechanical Engineering and Materials Science.
15. Terekhin AA, Sidelnikov RV and Terekhina TV. Numerical Analysis of The Influence of Surface Friction on Aerodynamic Characteristics of a Profile. Series "Mechanical Engineering".
16. Spalart PR and Allmaras SR. "A one-equation turbulence model for aerody-namic flows". AIAA J 92 (1992): 0349.
17. Hamdamov MM, Ishnazarov AI and Mamadaliev KA. "Numerical Modeling of Vertical Axis Wind Turbines Using ANSYS Fluent Software". Lecture Notes in Computer Science (including subseries Lecture Notes in Artificial Intelligence and Lecture, 13772 LNCS (2023): 156-170.
18. Khujaev IK, Fayziev RA and Hamdamov MM. "Numerical Solution of the Combustion Process Using the Computer Package Ansys Fluent". Lecture Notes in Computer Science (including subseries Lecture Notes in Artificial Intelligence and Lecture 13772 LNCS (2023): 26-37.
19. Hamdamov M., et al. "Axisymmetric turbulent methane jet propagation in a wake air flow under combustion at a finite velocity". IOP Conference Series: Materials Science and Engineering 1030.1 (2021): 012163
20. Khujaev IK and Hamdamov MM. "Axisymmetric turbulent methane jet Propagation in a co-current air flow under combustion at a finite velocity". Herald of the Bauman Moscow State Technical University 5 (2021): 89-108
21. Fayziev RA and Kurbanov FM. Mathematical modeling and forecasting of electricity production in enterprises of the energy system of Uzbekistan AIP Conference Proceedings 1 (2022): 020015.
22. Fayziev RA and Kurbanov FM. "Modeling and Forecasting of Net Income from the Country's Electricity Supply". ACM International Conference Proceeding Series (2021): 407-412.

Volume 5 Issue 6 December 2023